Investigation of Problems in Thermal Convection: Rigid Boundaries

J. R. HERRING

Goddard Institute for Space Studies, NASA, New York, N. Y.

(Manuscript received 15 January 1964)

ABSTRACT

An investigation of thermal convection in a thin layer of fluid has recently been reported (Herring, 1963). The calculation included only those nonlinearities having the form of an interaction of a fluctuating quantity with the mean temperature field. In addition, free boundary conditions were employed and the fluctuating velocity and temperature fields were composed of one horizontal wave number, α. In the present paper, the calculation is extended to include the effects associated with rigid boundaries and many horizontal wave numbers.

The results of the multi-α study indicate that the stable steady state solution contains only one α, provided the Rayleigh number, R, is less than $\cong 10^6$. Above $R \cong 10^6$, the stable solution contains at least two α's. The stable single-α solutions have a somewhat different value of α than either that predicted by the maximum heat flux principle of Malkus (1954) or that predicted by the relative stability criterion of Malkus and Veronis (1958). At present, we are not able to characterize the stability of the system by postulating an extremal for some simple property of the flow.

The value of the Nusselt number found here for rigid boundaries is $N = 0.115R^{\frac{1}{3}}$, for large R. This value for N is within $\sim$20 per cent of the experimental value for large Prandtl number fluids. The rms values of the velocity and temperature fluctuation fields computed here appear to have the form expected for large Prandtl number fluids. The lack of accurate experimental data prevents us from drawing definite conclusions as to the numerical accuracy for these quantities. The computed mean temperature profile is qualitatively correct, but develops a thin stabilizing region with a stable temperature gradient just exterior to the thermal boundary layer. It is concluded that the stabilizing region represents a self-adjustment in the flow which compensates for the omission of the effects of eddy processes on the equations of motion.

1. Introduction

In a previous paper (Herring, 1963: hereafter referred to as IPTC) the thermal convection equations for a thin layer of fluid were investigated numerically. The procedure used was to include only those nonlinear terms which describe the interaction of the mean temperature field with a velocity or temperature fluctuation. The terms omitted (the fluctuating interactions) were discarded in a manner consistent with the conservation properties of the fluid. The velocity and temperature fluctuations obeyed free boundary conditions on horizontal conducting surfaces. The numerical study was also limited to systems containing only one horizontal wave number.

In the present paper we extend the calculation to include systems containing many horizontal wave numbers and obeying rigid boundary conditions on the conducting surfaces. The numerical procedure employed in the present paper is similar to that used in IPTC. The equations of motion are Fourier analyzed and the Fourier components are allowed to evolve to their steady state values from arbitrary initial conditions. The present calculation differs from that of IPTC in that we set the Prandtl number, σ, equal to infinity. This choice of σ allows a simpler formulation of the problem in Fourier space and makes the transient behavior of the systems simpler. The steady state values of the amplitudes can be seen from the equations of motion to be independent of σ.

The solutions obtained in the present calculations for rigid boundaries and one horizontal wave number are qualitatively similar to the corresponding ones for free boundaries. The velocity and temperature profiles have a reasonable boundary layer structure and, at large Rayleigh number (=R), the Nusselt number is found to be proportional to $R^{\frac{1}{3}}$ provided the horizontal wave number, α, which supports the convection, is close to that which maximizes the heat transport. The most significant difference between the two calculations is that the rigid boundary system transports much less heat than the free boundary system. The use of rigid boundaries reduces the heat transport by a factor of 2.3. The heat transport for rigid boundaries, without the fluctuating interactions, is thus within 10 to 30 per cent of the experimental heat transport, for large Prandtl number fluids.

The multi-α systems were investigated at small and intermediate Rayleigh numbers ($R < 10^6$). For this range of Rayleigh numbers, the analysis indicated that

the stable steady state contains only one α. In this part of the investigation we include four α's to represent the fluctuating fields. These were allowed to evolve from arbitrary initial conditions to the steady state. In all cases investigated, the steady state so achieved contained at most only two of the initially excited horizontal wave numbers. However, those steady states which contained two α's were found to be unstable to perturbations of horizontal wave numbers situated between the wave numbers of the amplitudes surviving in the above steady state. After its introduction into the system, the perturbation was found to grow and eventually to replace one or the other of the original amplitudes. In this manner, it was possible to continue the calculation until a limiting, completely stable, wave number was identified with reasonable accuracy. This stable wave number turned out to be somewhat smaller than that which maximizes the total heat transport, and it transports about 20 per cent less heat than the latter. The $R^{\frac{1}{3}}$ law was found to be valid for both of the above solutions, for R larger than $\sim 10^4$.

The numerical study was supplemented by a linear stability analysis of the single-α solutions against infinitesimal disturbances at other α's. For moderate Rayleigh numbers ($R \lesssim 10^6$), the linear stability study gave stable solutions which were identical to those found from studies of systems containing many horizontal wave numbers. At large Rayleigh numbers, ($R \gtrsim 10^6$), the stability analysis indicates that a steady state must have at least two α's in order for it to be stable. The threshold for the occurrence of the double-α steady states is at $R \sim 10^6$. The numerical study at $R = 10^6$ indicates that these solutions have a strong component at a small α and a very weak component at roughly twice the α of the first component. This second component, however, makes a negligible contribution to the total heat transport at $R = 10^6$. At larger R, its contribution may become significant.

The occurrence of the multi-α steady state at large R is apparently connected with the use of rigid boundaries. For free boundaries, no such behavior was noted, up to a Rayleigh number of 10^6, although at larger R, several mode solutions may exist for the latter case also.

The results of the multi-α and stability studies may be used to test the principle of relative stability proposed by Malkus and Veronis (1958) and Malkus (1959). The latter principle asserts that the most stable, statistically steady solution is that which maximizes the square of the mean temperature gradient averaged throughout the volume of the fluid. This principle is independent of the conservative non-linearities in the equations of motion. Therefore, it should apply equally well to those equations which omit the fluctuating interactions as it does to the more realistic complete set of equations. Our results indicate that the stable solutions are not those that maximize $\langle\beta^2\rangle$. The stable solutions have a somewhat smaller value of α than that which maximizes $\langle\beta^2\rangle$. However, the difference between the two, as far as total heat transport is concerned, is not large ($\sim$20 per cent).

As pointed out in IPTC, the convective system which deletes the fluctuating interactions is very similar to a theory of convection proposed by Malkus (1954, 1960). In fact the system considered here is identical to a reformulation of the Malkus theory by Spiegel (1962) provided the wave numbers in the nonfluctuating system are adjusted so as to keep the mean temperature gradient everywhere nonnegative.

Our conclusions with regard to the Malkus theory for the present calculation are substantially the same as those stated in IPTC. We note, however, that the heat transport computed here for rigid boundaries is quite close to the experimental results (within 10–30 per cent). The present calculation therefore seems to have good quantitative accuracy as to its prediction for the total transport of heat. As for the detailed shape of the mean temperature profile its accuracy is probably not as satisfactory, although the lack of experimental data prevents us from drawing a definite conclusion on this point. The mean temperature profiles computed here develop an overshoot region just outside the boundary layer, in which a stabilizing gradient develops. This behavior is qualitatively the same as that found for the free boundary calculation.

2. Theory

a) The equations of motion and boundary conditions. We consider a thin layer of fluid confined between two perfectly conducting horizontal plates located at $z=0$ and $z=d$. The lower plate is maintained at zero degrees, and the top at a temperature $-T_0$ on an arbitrary temperature scale. The equations appropriate for our system are the Boussinesq approximation to the Navier-Stokes equations (Chandrasekhar, 1961). In writing these equations, it is convenient to split up the temperature field into its horizontal mean, $\bar{T}(z,t)$ and its fluctuation, $\Theta(\mathbf{r},t)$ from its horizontal mean. The heat transport equation then splits into two equations—one for Θ and one for $\bar{T}(z,t)$. The latter equation is conveniently written in terms of the mean temperature gradient, $\beta(z) \equiv -d\bar{T}/dz$. The equations of motion are written in a nondimensional form, in which the only parameters appearing are the Prandtl number, σ, and the Rayleigh number R. They are:

$$\nabla \cdot \mathbf{v} = 0 \tag{1}$$

$$\left(\frac{1}{\sigma}\frac{\partial}{\partial t} - \nabla^2\right)\nabla^2 \mathbf{v} = R\{\mathbf{k}\nabla^2 - \nabla\nabla\cdot\}\Theta + \frac{1}{\sigma}\nabla \times (\nabla \times \mathbf{v} \cdot \nabla \mathbf{v}) \tag{2}$$

$$\left(\frac{\partial}{\partial t} - \nabla^2\right)\Theta = \beta w - \nabla \cdot (\mathbf{v}\Theta - \mathbf{k}\overline{w\Theta}) \tag{3}$$

$$\left(\frac{\partial}{\partial t}-\frac{\partial^2}{\partial z^2}\right)\beta=+\frac{\partial^2}{\partial z^2}\overline{w\theta}, \tag{4}$$

where

$$\beta(z,t)\equiv-\frac{\partial\bar{T}}{\partial z}(z,t) \quad \text{and} \quad \mathbf{v}=(U,V,W).$$

In equations (1)–(4), $-\mathbf{k}$ denotes the direction of gravity and the bars in equations (3) and (4) denote an average over the horizontal. Equation (2) is the double curl of the momentum equation; hence the pressure variable is absent. The nondimensional variables $(\mathbf{v},\Theta)$ are related to the dimensional ones (denoted by primes) in the following way:

$$\mathbf{v}=\frac{d}{\kappa}\mathbf{v}'$$

$$T=T'/T_0.$$

We have chosen the units of length to be the distance, d, between the confining plates and the unit of time to be d^2/κ, where κ is the thermometric diffusivity of the fluid.

The boundary condition on the velocity field $\mathbf{v}$ is that it vanishes on the conducting surfaces located at $z=0$ and $z=d$. The continuity equation, (1), then implies that the first vertical derivative of the vertical component of the velocity, W, vanishes on the surfaces. In the nondimensional notation the boundary conditions are

$$W(0,t)=\frac{\partial W}{\partial z}(0,t)=W(1,t)=\frac{\partial W}{\partial z}(1,t)=0, \tag{5}$$

$$\Theta(0,t)=\Theta(1,t)=0, \tag{6}$$

and

$$T(0,t)=0, \quad \text{and,} \quad T(1,t)=-1.$$

The boundary conditions on Θ follow from its definition as the fluctuation from a horizontal mean, and from the fact that the confining surfaces at $z=0$ and 1 have infinite conductivity.

The last terms on the right hand side of (2) and (3), have the form of the deviation of a bilinear quantity from its horizontal average (fluctuating interactions). By deleting these terms and assuming $\sigma\to\infty$, we obtain the system to be investigated:

$$\nabla^4 W=-R\nabla_1^2\Theta \tag{7}$$

$$\left(\frac{\partial}{\partial t}-\nabla^2\right)\Theta=\beta W \tag{8}$$

$$\left(\frac{\partial}{\partial t}-\frac{\partial^2}{\partial z^2}\right)\beta=-\frac{\partial^2}{\partial z^2}\overline{W\Theta}, \tag{9}$$

where

$$\nabla_1^2=\frac{\partial^2}{\partial x^2}+\frac{\partial^2}{\partial y^2}.$$

There are two more equations for U and V which should be included in (7), but in the absence of the fluctuating self-interactions these are not necessary to make the set (7)–(9) complete. In writing (7) we have put the Prandtl number σ equal to infinity. This choice of σ eliminates the time derivatives occurring in equation (2). We note also that equation (7) is the exact momentum equation for $\sigma\to\infty$, since the non-linear term disappears in this limit.

We shall refer hereafter to the system described by (7)–(9) as the "nonfluctuating" system, in order to distinguish it from the real physical system which includes the fluctuating interactions. This choice of terminology is motivated by the fact that in (7) and (9) the fluctuating interactions are omitted, and by the fact that the resulting system does not fluctuate in time.

The physical significance of omitting the fluctuating interactions is discussed in IPTC. Here we simply note that their omission leads to no nonphysical results; the system (7)–(9) obeys the same conservation laws as does the complete system and the energy spectrum associated with (7)–(9) is positive definite. We also refer the reader to IPTC for a discussion of the qualitative behavior of the nonfluctuating system. The observations made there for the free boundary system are presumably valid for the rigid boundary system also.

b) Fourier decomposition of the equations. It is convenient to work with the Fourier components of (7) and (9) rather than their space variable form. To this end, we write:

$$W(\mathbf{r},t)=\pi^2\sum_\alpha f_\alpha(x,y)W_\alpha(z)$$

$$\Theta(\mathbf{r},t)=\sum_\alpha f_\alpha(x,y)\Theta_\alpha(z).$$

Here $\{f_\alpha(x,y)\}$ is a set of orthonormal functions generated by the operator ∇_1^2 and obeying periodic boundary conditions in the horizontal:

$$\nabla_1^2 f_\alpha(x,y)=-\pi^2\alpha^2 f_\alpha(x,y),$$
$$|f_\alpha^* f_{\alpha'}|=\delta_{\alpha\alpha'}.$$

Substituting the above representation into (7) gives

$$\left(\frac{\partial^2}{\partial z^2}-\pi^2\alpha^2\right)^2 W_\alpha(z)=R\alpha^2\Theta_\alpha(z). \tag{10}$$

We may solve (10) for $W_\alpha(z)$ in terms of a given $\Theta_\alpha(z)$ by constructing the appropriate rigid boundary Green's function, $G(z|z')$:

$$W_\alpha(z)=\frac{R\alpha^2}{\pi^4}\int_0^1 G_\alpha(z|z')\Theta_\alpha(z')dz', \tag{11}$$

where

$$\left(\frac{d^2}{dz^2}-\pi^2\alpha^2\right)^2 G(z|z')=\pi^4\delta(z-z').$$

Here, $G(z|z')$ satisfies the rigid boundary conditions given by equation (5). The calculation of $G(z|z')$ is given in Appendix A.

The boundary conditions on Θ and β given by (6) permit us to write Θ_α as a sine series and $\beta(z,t)$ as a cosine series:

$$\Theta_\alpha(z)=\sum_1^\infty \Theta_n{}^\alpha \sin n\pi z \tag{12}$$

$$\beta(z,t)=1+\sum_1^\infty \beta_n \cos n\pi z. \tag{13}$$

Introduction of (11), (12) and (13) into the equations of motion, (8) and (9), gives the following equation for $\Theta^\alpha{}_n$ and β_n:

$$\left(\frac{\partial}{\partial\tau}+n^2+\alpha^2\right)\Theta_n{}^\alpha = W_n{}^\alpha+\frac{1}{2}\sum_{m=1}^\infty(\beta_{|n-m|}-\beta_{n+m})W_m{}^\alpha \tag{14}$$

$$\left(\frac{\partial}{\partial\tau}+n^2\right)\beta_n = -n^2-\sum_2^{\pi^2}\sum_{m=1}^\infty\sum_\alpha W_m{}^\alpha(\Theta_{n+m}{}^\alpha+\sigma(m-n)\Theta_{|m-n|}{}^\alpha), \tag{15}$$

where,

$$W_n{}^\alpha\equiv 2\int_0^1 \sin n\pi z w_\alpha(z)dz,$$

$$\sigma(x)=1,\quad x>0$$
$$=0,\quad x=0$$
$$=-1,\quad x<0,$$

and

$$\tau=\pi^2 l.$$

The velocity amplitude $W_n{}^\alpha$ is related to the temperature fluctuation field $\Theta^\alpha{}_n$ through equation (11):

$$W_n{}^\alpha=\frac{R\alpha^2}{\pi^4}\sum_1^\infty G_{n,m}\Theta_m{}^\alpha, \tag{16}$$

where the symmetric Green's matrix, G, is given by:

$$G_{n|m}=2\int_0^1\int_0^1 dzdz' \sin n\pi z \sin m\pi z' G(z|z')$$
$$=\frac{1}{(n^2+\alpha^2)^2}\delta_{n,m}$$
$$-\frac{4nm\alpha[(-1)^{n+m}+1]}{\pi(n^2+\alpha^2)^2(m^2+\alpha^2)^2}\frac{(-1)^n\cosh\pi\alpha-1}{(-1)^n\sinh\pi\alpha-\pi\alpha}. \tag{17}$$

For the derivation of this, we refer the reader to the Appendix.

The total heat transported by the system in the steady state, N, is given by the mean temperature gradient evaluated at the lower boundary. According to equation (13) it is

$$N=1+\sum_1^\infty \beta_n. \tag{18}$$

The conservation properties of the rigid boundary system are the same as for the free boundary system:

$$\sum_{n,\alpha}\left\{\frac{\partial}{\partial\tau}(\Theta_n{}^\alpha)^2+(n^2+\alpha^2)(\Theta_n{}^\alpha)^2\right\}+\sum_n\left\{\frac{\partial}{\partial\tau}\left(\frac{\beta_n}{n}\right)^2+\beta_n{}^2\right\}=\sum_{n,\alpha}W_n{}^\alpha\Theta_n{}^\alpha \tag{19}$$

$$\sum\frac{\partial}{\partial\tau}\left(\frac{\beta_n}{n^2}\right)+N(t)=\frac{\pi^2}{2}\sum_{n,\alpha}W_n{}^\alpha\Theta_n{}^\alpha+1. \tag{20}$$

Equation (19) expresses the conservation of entropy, and (20) expresses the constancy of total energy flux, in the steady state. These equations are directly derivable from (14) and (15).

3. Procedure

Our procedure for solving (14) and (15) is to assign an initial set of amplitudes to Θ_n and β_n and allow the system to evolve to its statistically steady state. This method guarantees the stability of the steady state, provided a sufficient range of initial data is sampled. In performing the numerical integration, we discard those amplitudes which we anticipate will be zero in the steady state. Since the steady state form of $\Theta_\alpha(z)$ has even parity about the midpoint $z=\frac{1}{2}$, we may discard its even sine modes. Inspection of (15) then shows that we may discard the odd cosine modes of β_n. Defining

$$\Theta^\alpha{}_{2n-1}=\theta^\alpha{}_n$$
$$\beta_{2n}=\tilde{\beta}_n$$
$$W^\alpha{}_{2n-1}=w^\alpha{}_n$$

then allows us to abbreviate the system as follows:

$$w_n{}^\alpha=\frac{R\alpha^2}{\pi^4}\sum_m g_{mn}\theta_m \tag{21}$$

$$\left\{\frac{\partial}{\partial\tau}+[(2n-1)^2+\alpha^2)]\right\}\theta_n{}^\alpha = w_n{}^\alpha+\tfrac{1}{2}\sum_m(\tilde{\beta}_{|n-m|}-\tilde{\beta}_{n+m-1})w_m{}^\alpha \tag{22}$$

$$\left(\frac{\partial}{\partial\tau}+4n^2\right)\bar{\beta}_n = -2\pi^2n^2\sum_{m,\alpha} w_m{}^{\alpha}[\theta_{n+m}{}^{\alpha}+\sigma(m-n-\tfrac{1}{2})\theta_{|n-m+\frac{1}{2}|+\frac{1}{2}}], \tag{23}$$

where,

$$g_{nm}=\frac{\delta_{mn}}{[(2n-1)^2+\alpha^2]^2} - \frac{16\alpha(2n-1)(2m-1)}{\pi[(2n-1)^2+\alpha^2]^2[(2m-1)^2+\alpha^2]^2}\frac{\cosh^2\pi\alpha/2}{\sinh\pi\alpha+\pi\alpha}. \tag{24}$$

In practice, it is necessary to truncate the above infiinite set of equations. Our procedure in this matter is to set all θ_n and w_n modes above a certain integer, n_0, equal to zero. Equation (23) then implies that all $\bar{\beta}_n$ are zero if $n\geq 2n_0-1$. This method of truncating the system guarantees that the approximate system satisfies the exact conservation equations for entropy and heat flux. We note, however, that $\bar{\beta}_n$'s will have appreciable truncation errors if $n>n_0$.

In most of the numerical calculations, we disregard the time derivative in equation (23) for $\bar{\beta}_n$, thus putting the mean temperature field in instantaneous equilibrium with the velocity and temperature fluctuation fields. This procedure greatly hastens the convergence to the steady state, and a few runs with the time derivatives present indicate that no unstable steady states evolve from this procedure.

In the numerical calculation of the temperature fields $\theta^{\alpha}(z)$ and $\beta(z)$, we use their sine and cosine representations, given by (12) and (13). For the velocity field, it is convenient to use a set of functions, $\varphi_n(z)$, which satisfy the velocity boundary conditions. According to equations (11), (12) and (A5) we may write

$$W^{\alpha}(z)=\frac{R\alpha^2}{\pi^4}\sum_{1}^{\infty}\varphi_n(z)\theta_n{}^{\alpha}$$

where

$$\varphi_n(z)=\sin(2n-1)\pi z - \frac{(2n-1)\pi\{z\sinh\pi\alpha(1-z)+(1-z)\sinh\pi\alpha z\}}{\sinh\pi\alpha+\pi\alpha}. \tag{25}$$

By using the set of functions $\varphi_n(z)$ to represent the velocity field, we automatically force the truncated system to satisfy the rigid boundary conditions at any arbitrary order of truncation n_0.

4. Results

a) Single-α amplitudes. The steady state single α amplitudes are shown in Figs. 1–8 for a range of Rayleigh numbers extending from $R=4\times10^3$ to $R=10^6$. The normalization of W and Θ is given in the figure captions, while $\bar{T}(z)$ requires no normalization. The values of α in Figs. 1–8 are approximately those for which the system is stable against small perturbations at other wave numbers. The method of determining this α is given in Section 4b. The characteristic shape of these curves is the same over a wide range of wave numbers, and their numerical values would not be appreciably altered if α were changed to that wave number which maximizes the total heat transport. At low Rayleigh numbers ($R\lesssim 4\times10^3$) we expect the calculations to have good quantitative accuracy even as to the detailed shape of the profiles.

The amplitudes shown in Figs. 1–8 are qualitatively very similar to those computed in IPTC for free boundaries. The physical interpretation of the features of these curves as given in IPTC applies to the rigid boundary calculation as well. The main quantitative difference between the two calculations is traceable to the fact that the rigid boundary system has a lower heat transport, so that the boundary layer is more extensive. At large R, we notice that the mean temperature gradient, β, becomes slightly negative in a region near

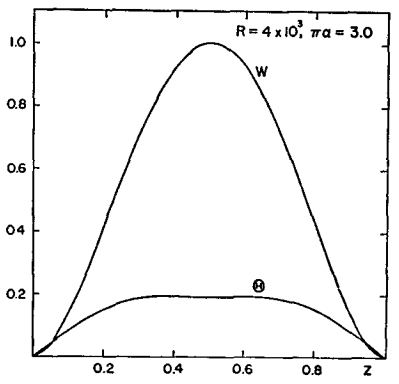

FIG. 1. $0.105W$ and 0.939Θ for $R=4\times10^3$ and $\pi\alpha=3.00$.

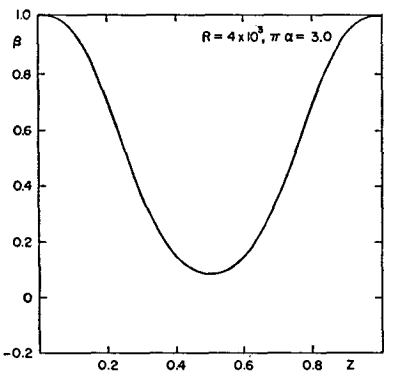

FIG. 2a. Mean gradient, $\beta(z)$, for $R=4\times10^3$ and $\pi\alpha=3.0$. $\beta(z)$ is normalized by the total heat transport, $N=1.968$.

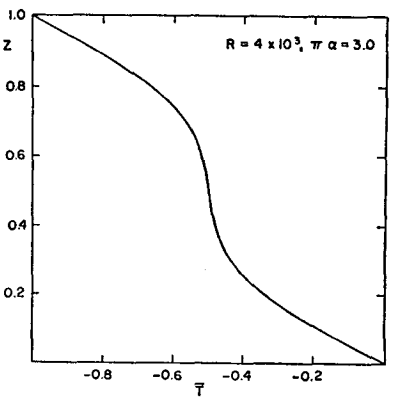

FIG. 2b. Mean temperature $\bar{T}(z)$ for $R=4\times10^3$ and $\pi\alpha=3.0$.

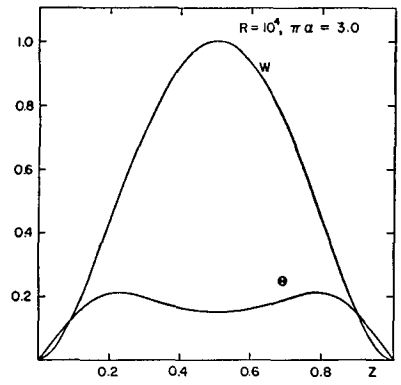

FIG. 3. $4.56\times10^{-2}W$ and 1.13Θ for $R=10^4$ and $\pi\alpha=3.0$.

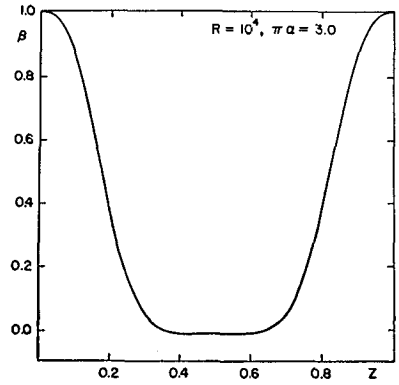

FIG. 4a. Mean gradient, $\beta(z)$, for $R=10^4$ and $\pi\alpha=3.0$. $\beta(z)$ is normalized by the total heat transport $N=2.824$.

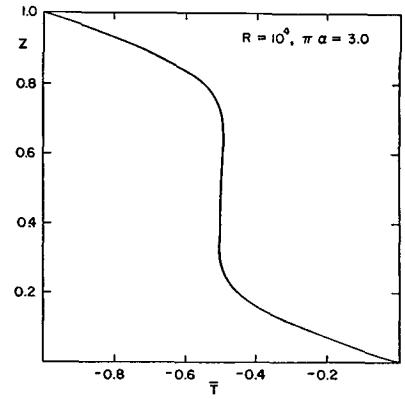

FIG. 4b. Mean temperature, $\bar{T}(z)$, for $R=10^4$ and $\pi\alpha=3.0$.

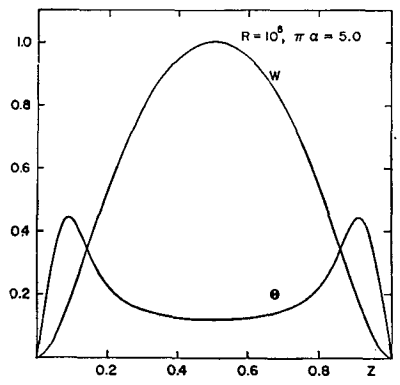

FIG. 5. $7.85\times10^{-3}W$ and 2.232Θ for $R=10^5$ and $\pi\alpha=5.0$.

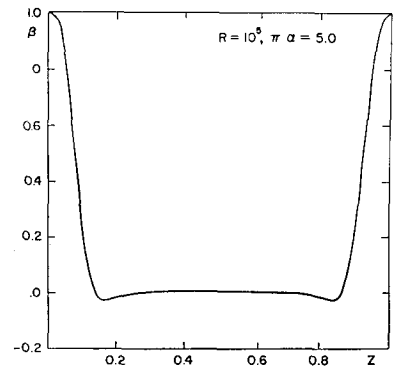

FIG. 6a. Mean gradient, $\beta(z)$, for $R=10^5$ and $\pi\alpha=5.0$. $\beta(z)$ is normalized by the total heat transport, $N=6.712$.

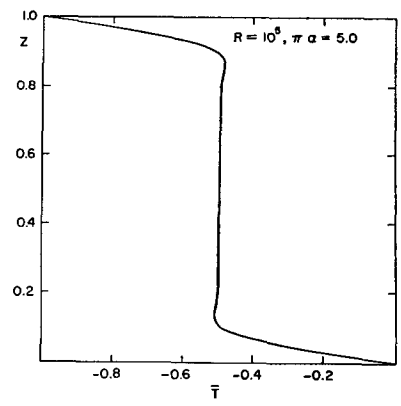

FIG. 6b. Mean temperature, $\bar{T}(z)$, for $R=10^5$ and $\pi\alpha=5.0$.

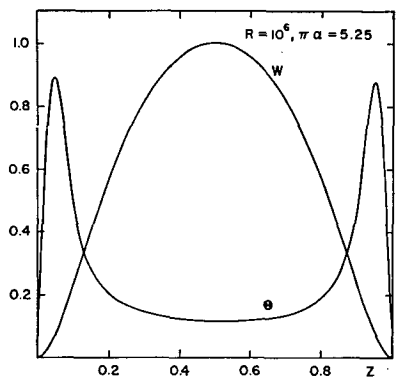

FIG. 7. $1.91\times10^{-3}W$ and 4.80Θ for $R=10^6$ and $\pi\alpha=5.25$.

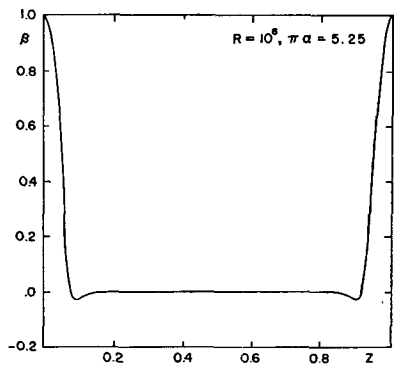

FIG. 8a. Mean gradient, $\beta(z)$, for $R=10^6$ and $\pi\alpha=5.25$. $\beta(z)$ is normalized by the total heat transport, $N=11.53$.

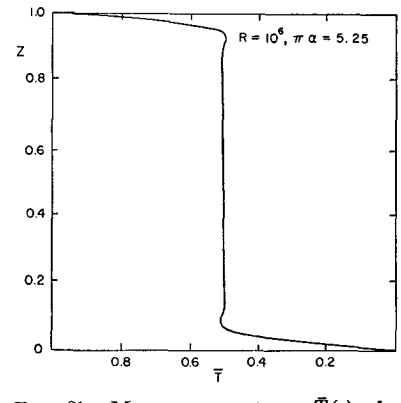

FIG. 8b. Mean temperature, $\bar{T}(z)$, for $R=10^6$ and $\pi\alpha=5.25$.

the boundary (see Figs. 2, 4, 6 and 8), and extremely small, but positive, in the mid-region of the flow. The presence of a thin negative β region was noted for the free boundary calculations also, and we interpret it as an overshoot phenomenon, characteristic of convective systems of large horizontal scale. For systems having a small horizontal scale, this behavior disappears. However, for the latter system, the convective heat transport in the central region is rather small.

The velocity fields given in Figs. 1, 3, 5 and 7 are dominated by their first mode, $\varphi_1(z)$ [equation (25)], with the higher harmonics contributing only a few per cent to the total amplitude, even at large Rayleigh numbers. As noted in IPTC, this behavior is attribut-

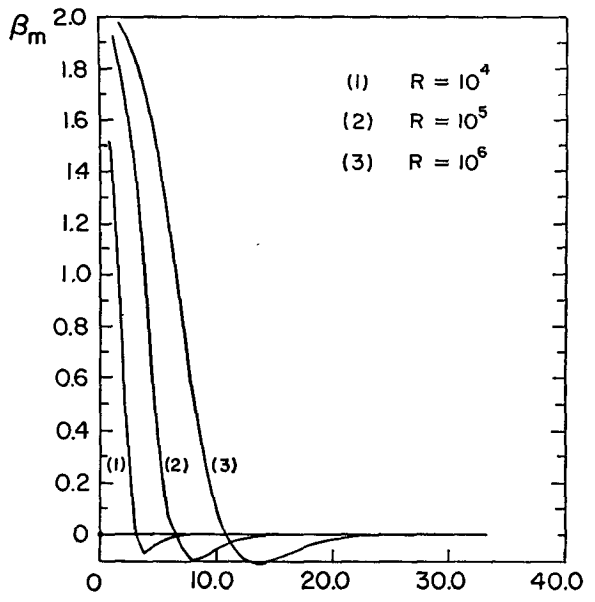

FIG. 9. Cosine spectrum of the mean temperature gradient for $R=10^4$, 10^5, and 10^6. The values of $\pi\alpha$ for a given R are the same as in the preceding figures.

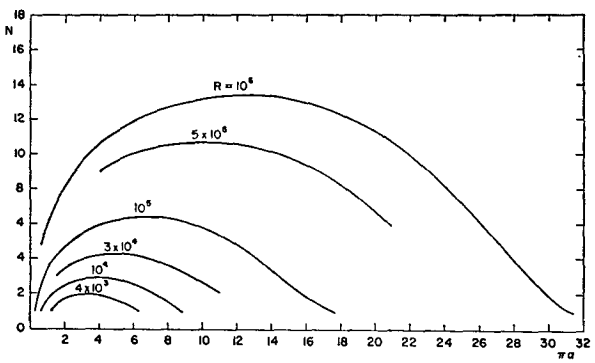

FIG. 10. The total heat transport, N, as a function of α. The values of R are given in the figure.

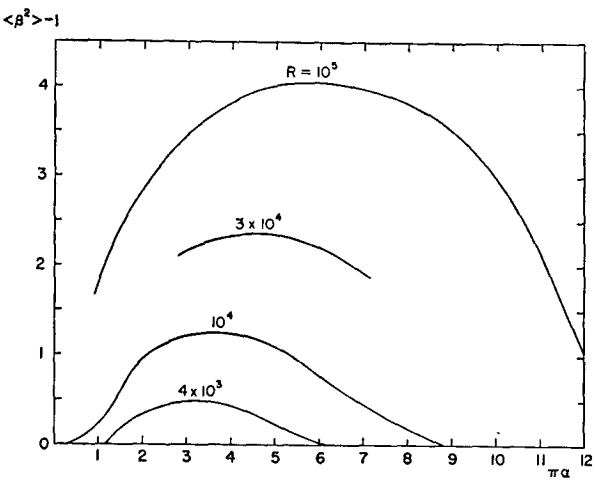

FIG. 11. $\langle\beta^2\rangle-1$ as a function of α. The values of R are given in the figure.

able to the fact that the velocity field is marginally stable on the mean distorted temperature field. The fact that the velocity field is composed largely of its first mode indicates the character of the nonlinear coupling in our system. Thus the small scale motions receive most of their energy through the interaction of the large scale motions with distortions in the mean temperature field. They lose most of their energy by conduction. The large scale motions, on the other hand, are quite close to being marginally stable on the large scale part of the mean temperature field.

The cosine spectrum of the mean temperature gradient, β, is given in Fig. 9 for $R=10^4$, 10^5, 10^6. The values of α in these graphs are the same as for the amplitudes presented in Figs. 1–8. We have connected the points with a smooth curve for the sake of clarity. The tendency for the lower modes to saturate at $\bar{\beta}_n=2$ corresponds to the extremely small gradient outside the boundary layer. At the larger Rayleigh numbers, the spectrum is nearly Gaussian at small n, and decreases more rapidly at large n. The region of negative $\bar{\beta}_n$'s is produced by the rigid boundary conditions, and is not present for the free boundary calculations given in IPTC. At extremely large n, the $\bar{\beta}_n$ spectrum decays exponentially to zero.

The total heat transport as a function of R and α is given in Fig. 10. The Rayleigh numbers are given in the figure. These curves are qualitatively similar to the free boundary calculations, but the value of α which maximizes the heat transport increases more rapidly as a function of R for rigid boundaries than for free boundaries. This value of α begins at 0.99 at critical Rayleigh number ($R=1708$), and increases approximately linearly with $R^{\frac{1}{3}}$. At large R, the value of α which maximizes the total heat transport is well represented by[1]

$$\pi\alpha_m\cong3.1+0.096(R-1708)^{\frac{1}{3}}. \tag{26}$$

In discussions of the relative stability criterion of Malkus and Veronis, it is necessary to have $\langle\beta^2\rangle$, the average of the square of β. Fig. 11 gives $\langle\beta^2\rangle$ for a range of α and R. The principle of relative stability asserts that the most stable solution is that which maximizes $\langle\beta^2\rangle$. According to Fig. 11, the value of α which maximizes $\langle\beta^2\rangle$ is given by,

$$\pi\alpha_{RS}\cong3.1+0.074(R-1708)^{\frac{1}{3}}. \tag{27}$$

It should be noted that both the above principles (the principle of maximum heat transport, and the principle of maximum $\langle\beta^2\rangle$) have an $R^{\frac{1}{3}}$ law for the Nusselt number at large R. This is shown in Fig. 12. The curve marked N_s gives the heat transported by the stable

[1] Equation (26) is intended to represent the dependence of α_m on R only over the range of R covered by the present calculation ($R\lesssim10^6$). At larger R this dependence may become weaker than $R^{\frac{1}{3}}$. Preliminary investigations of the free-boundary problem at $R=10^{10}$ indicate that $\alpha_m(R)$ does in fact have a weaker dependence on R than $R^{\frac{1}{3}}$, at extremely large R.

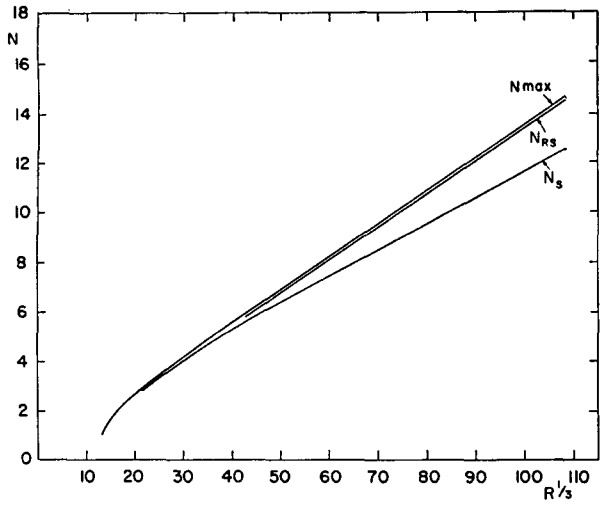

FIG. 12. Heat transport, N, as a function of $R^{\frac{1}{3}}$. N_{max} is the maximum value of N for a given R. N_{RS} is the heat transport as predicted by the relative stability criterion, and N_S is the heat transported by the stable single-α solutions.

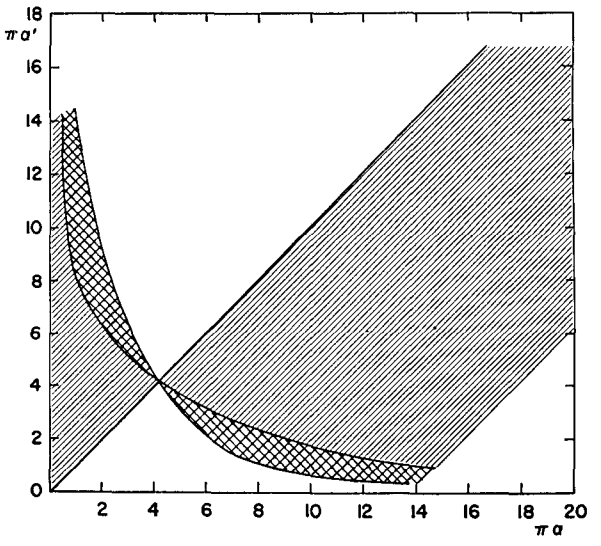

FIG. 13. Stability diagram for $R=10^5$. α is the wave number that supports the convection and α' is the wave number of the small perturbation.

single-α solutions to be discussed in the next section. For $R \gtrsim 10^4$ the principle of maximum heat transport gives

$$N=0.135R^{\frac{1}{3}} \tag{28}$$

while the principle of maximum $\langle\beta^2\rangle$ gives

$$N=0.133R^{\frac{1}{3}}. \tag{29}$$

b) Stability of the single-α solutions. The solutions obtained in the preceding sections are stable against arbitrary perturbations of the same horizontal wave number for which the fields were computed. This stability is inherent in the integration methods used to obtain these solutions. The stability against disturbances of wave numbers α', other than that wave number which supports the convection process, has not yet been assured and we investigate here the case of small amplitude disturbances. We suppose that small disturbances $\delta w_n{}^{\alpha'}$ and $\delta\theta_n{}^{\alpha'}$ are introduced into the steady state system θ^α, w^α, and β. According to equations (21), (22), and (23), $\delta\theta^{\alpha'}$ satisfies the following equation:[2]

$$\left(\frac{\partial}{\partial\tau}+\triangle\right)\delta\theta^{\alpha'}=R\alpha'^2B(\beta)g\delta\theta^{\alpha'}. \tag{30}$$

Here, $\delta\theta^{\alpha'}$ is the vector $(\delta\theta_1{}^{\alpha'},\delta\theta_2{}^{\alpha'},\cdots)$ and $\triangle$ and B are the following matrices:

$$\triangle=(n^2+\alpha'^2)\delta_{nm}$$
$$B(\beta)=\delta_{nm}+\tfrac{1}{2}(\bar{\beta}|_{n-m}|-\bar{\beta}_{n+m-1}).$$

g is the Green's function matrix given by equation (24). In this analysis, $\delta\theta^{\alpha'}$ and $\delta w^{\alpha'}$ are assumed to be so small that we may neglect their quadratic terms which modify the mean temperature gradient, β. Since (30) is linear, it has solutions

$$\delta\theta^{\alpha'}=e^{\eta t}\psi$$

where,

$$(\eta+\triangle)\psi=RB(\beta)g\psi. \tag{31}$$

The steady state solutions (θ, w, and β) will be stable if all eigenvalues, η, have negative real parts. It should be noted that η depends on α' through Δ and g, and for complete stability, the $\eta(\alpha')$'s should be nonpositive for all α'.

For free boundaries it follows from a theorem of Spiegel (1962) that the eigenvalues, η, all have negative real parts if the following condition is met:

$$R\leq R_c(\alpha'), \text{ for all } \alpha'. \tag{32a}$$

Here R_c is the smallest eigenvalue of

$$\triangle\psi=R_c\alpha'^2B(\beta)g\psi. \tag{32b}$$

For free boundaries, g consists of only the first member of equation (24), and is diagonal. The case of $\alpha=\alpha'$ is quite difficult to analyze, because linear perturbations on the mean field β are induced. However, for $\alpha=\alpha'$, (32b) is the same equation satisfied by θ^α, so that stability in this case is ensured by the integration technique.

For rigid boundaries, there exists no proof that condition (32) implies stability, unless the B (β) matrix is unity. The difficulty is that for rigid boundaries, g is not diagonal, and equation (31) cannot be put into a generalized Hermitian form, which is a necessary step in the proof of the exchange of stabilities. In the present analysis, we assume without proof that the mean temperature field is such that condition (32) implies complete stability.

[2] The stability analysis discussed here assumes that $\sigma\to\infty$.

The calculation of the eigenvalue $R_c(\alpha')$ is conveniently carried out by means of a standard iteration technique (Hildebrand, 1962). Thus,

$$\frac{1}{\alpha'^2 R_c} = \lim_{n\to\infty} \frac{\langle\chi|A^n|\chi\rangle}{\langle\chi|A^{n-1}|\chi\rangle}, \tag{33}$$

where,

$$A = \triangle^{-1} B g.$$

In (33), χ is a trial vector which we may conveniently take as,

$$|\chi\rangle = (1,0,0,\cdots).$$

The iteration method converges quite rapidly because of the structure of the matrix g.

Fig. 13 gives the results of the stability analysis for $R=10^5$. In this figure, the shaded and crosshatched areas indicate the region for which $R_{\alpha'}<R$. α is the wave number which supports the convection, and α' is the wave number of the small perturbation. The unstable regions are bounded by lines of marginal stability. The point, α_s' at which the two lines of marginal stability cross is that wave number for which the single-α system is completely stable to small perturbations of any wave number α'.

The calculations at lower Rayleigh numbers are qualitatively similar to that shown in Fig. 13; they all indicate an α_s for which the single-α system is completely stable.

The crosshatched regions in Fig. 13 are zones of (α,α') in which there exist steady state solutions composed of two distinct α-modes, θ^α, and $\theta^{\alpha'}$. We may infer the existence of these solutions by the following experiment. First, we assume that a single-α solution has developed to its steady state, θ^α. A small but arbitrary perturbation $\delta\theta^{\alpha'}$ is then introduced into the system, and we suppose that $\delta\theta^{\alpha'}$ initially grows. The system, $\theta^\alpha+\delta\theta^{\alpha'}$ may now develop into a single α' mode, with θ^α decaying to zero, or it may develop into a two mode system, with θ^α and $\theta^{\alpha'}$ having finite amplitude. If the first alternative is achieved, the point (α',α) must lie in the stable, unshaded region in Fig. 13. If, on the other hand, (α',α) is also in the unstable zone, we conclude that the steady state system contains both modes, θ^α, and $\theta^{\alpha'}$. The crosshatched regions are then zones in which both (α,α') and (α',α) are in the unstable region. This region is vanishingly small at $R=10^4$, and grows with increasing R. We investigate the stability of these two mode solutions in Section 4c.

The calculated $\alpha_s(R)$ is given in Fig. 14, for $R\lesssim 5\times10^5$. The value of α_s is 3.11 at the critical Rayleigh number ($R=1708$), and increases monotonically with increasing R. The heat transported by these stable solutions is given by the curve marked N_s in Fig. 12.

Above $R=\cong 10^6$, the linear analysis indicates that there are no stable single-α solutions. This fact is illustrated in Fig. 15, which gives the $R_{\alpha'}$ for $\pi\alpha=5.3$, and $R=10^6$. In this case, the $R_{\alpha'}$ curve drops below R in two separate disconnected ranges of α'. At smaller R, the corresponding curves have no secondary minimum at the larger α', but are distorted—in the range of large α'—in such a manner as to make the appearance of a secondary minimum a consequence of increasing R above some threshold value. The value of this threshold lies between 5×10^5 and 10^6; we have not located it more accurately at present. The stability analysis at $R=10^6$ is given in Fig. 16.

c) Multi-α results. The analysis of the preceding paragraphs has permitted an identification of the stable, single-α solutions to the equations of motion (21), (22) and (23). In addition to these single-α solutions, there may also be multi-α solutions, which are stable against small perturbations. In fact, the stability analysis has

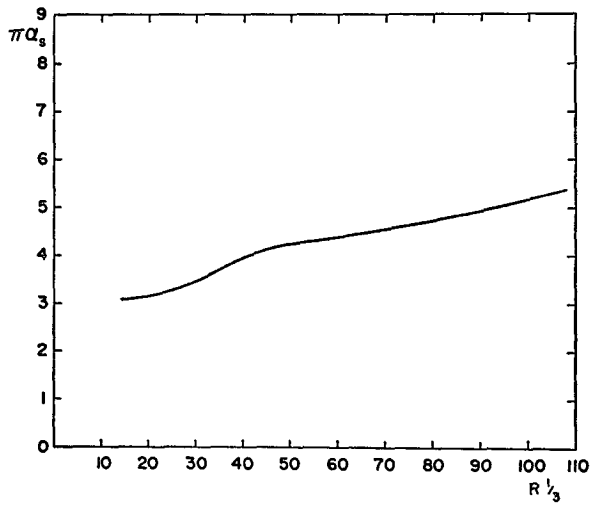

FIG. 14. Horizontal wave number, $\pi\alpha_s$, of the single—α stable solutions as a function of $R^{\frac{1}{3}}$.

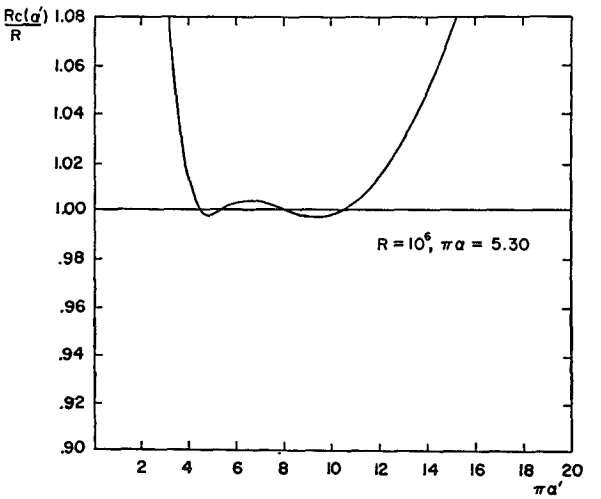

FIG. 15. Critical wave number, $R_c(\alpha')$ for $R=10^6$ and $\pi\alpha=5.25$. α' is the wave number of the small perturbation.

already indicated that solutions with two α's exist in a restricted region of (α,α'), although the stability of these double-α solutions has not yet been investigated. To investigate the possibility of multi-α solutions, we introduce a set of arbitrary amplitudes, $\theta^{\alpha i}$, as initial data into equations (21), (22) and (23), and allow the system to evolve to its steady state. The results of this phase of the investigation indicates that for $R \lesssim 10^6$ there are no stable multiple-α solutions.

The numerical integrations of the multi-α system indicate that it evolves either into a single or double-α steady state. The double-α steady states may occur if two of the α's lie in crosshatched regions as shown in Fig. 13. However these double-α solutions are not stable to disturbances of wave number between the α's of the double-α steady state. In the following paragraphs, we give two examples of the multi-α study; one case in which a single α survives to form a steady state, and the second in which two α's form a steady state of the unstable sort mentioned above. In these two examples, we discard the time derivative of β. The transient behavior of the system is shown only to illustrate the stability properties of the system.

Fig. 17 displays the evolution of a multi-α system for $R=10^4$. This figure shows the development of the first sines modes, $\theta_1{}^{\alpha}i$, for a group of 4 wave numbers, $\pi\alpha=$ 2, 3, 4 and 5. The total heat transport $N(t)$ is also given in Fig. 17. The scale for N is given to the right of the figure. The initial conditions are $\theta_1{}^{\alpha}i(t=0)=0.10$, and $\theta_n{}^{\alpha}i=0$, for $n>1$. We observe that the modes with $\pi\alpha=2$, 4 and 5 decay to zero with only the $\pi\alpha=3$ mode surviving in the steady state. That the mode with $\pi\alpha=3$ survives may be partially anticipated from the linear stability analysis, since the stable single-α solution at $R=10^4$ has $\pi\alpha=3.2$. The time scale for the relaxation of this system is long compared to the growth rate of any of the modes from the conduction state ($\tau\simeq 0.11$ for $\pi\alpha=3.0$). It is interesting to observe that the mode $\pi\alpha=4$ actually increases initially, and decays only after the total heat transport has almost relaxed to its steady state value.

As a second example of a multi-α system, we select the double-α system for which $\pi\alpha_1=1.7$, $\pi\alpha_2=8.0$, and $R=10^5$. According to the stability analysis (see Fig. 13), this system should develop into a double-α steady state. Its evolution from the initial conditions $\theta_1{}^{\alpha_1}=\theta_1{}^{\alpha_2}=0.1$, $\theta_n{}^{\alpha}i=0, n>1$ is given in Fig. 18. The amplitude of the α_2 mode appears to be concentrated more strongly in the boundary region than the α_1 mode, which has a relatively large amplitude in the body of the fluid. The Nusselt number for the combined system is 5.53, as compared to 4.35 and 6.30 for the single-α systems at $\pi\alpha=1.7$ and $\pi\alpha=8.0$, respectively.

The stability analysis for the above double-α system is given in Fig. 19. The system is apparently unstable to any small perturbations whose value of α is between α_1 and α_2. The development of the system subsequent to an introduction of a small disturbance at $\pi\alpha=3.2$ is shown in the right hand portion of Fig. 18.

As observed earlier, there appear to be no stable single-α solutions for $R \gtrsim 10^6$. The results of the stability analysis (Fig. 15) suggest that for R larger than some critical value $\sim 10^6$, the stable steady state consists of two distinct α-modes. The numerical studies of multi-α systems at $R=10^6$ indicate that the mode having the smaller α achieves a relatively large amplitude, with the mode of larger α contributing only a negligible amount to the advective heat transport. For example, at $R=10^6$, and $\pi\alpha_1=5.25$, $\pi\alpha_2=9.50$, $\theta_1{}^{\alpha_2}/\theta_1{}^{\alpha_1} \cong 0.465 \times 10^{-2}$. The mean temperature profile for the above two component system is only negligibly changed by the presence of the second mode at $\pi\alpha=9.5$. At larger Rayleigh numbers, this second mode (as well as others) may become significant. These results for large R are preliminary—a more detailed and extensive study will be undertaken as more appropriate numerical techniques are developed.

d) Some comments on the relative stability criterion of Malkus and Veronis. The stable single-α solutions described in the preceding section are not those for which $\langle\beta^2\rangle$ is maximum (cf. Figs. 11 and 14). These results are therefore counter-examples to the relative stability criterion proposed by Malkus and Veronis (1958) and Malkus (1959). This principle is based on certain integral properties of the equations of motion; it is therefore necessary to inquire why it is not applicable to the nonfluctuating system considered here. The fact that it is not valid for the nonfluctuating system would appear to vitiate its usefulness in any discussion of the stability properties of the complete convection equations.

As applied to the system investigated here, the relative stability criterion asserts that a particular solution, w^{α}, θ^{α}, and β_{α} is stable with respect to a small disturbance having the form of another solution, $\delta w^{\alpha'}=Aw^{\alpha'}, \delta\theta^{\alpha'}=A\theta^{\alpha'} (A \ll 1)$, provided $\langle\beta_{\alpha}{}^2\rangle > \langle\beta_{\alpha}{}^{2'}\rangle$[3]. Here $\beta_{\alpha'}$ is the mean temperature gradient which the fields $Aw^{\alpha'}$ and $A\theta^{\alpha'}$ would support if they had finite amplitude, $A=1$. We assume in the following discussion that the eventual state of the system consists of only one of the wave numbers, α or α', but not both.

The relative stability criterion is based on the fact that at the instant the disturbance $A\theta^{\alpha'}$ is introduced into the system,

$$\frac{d}{d\tau}\langle|\delta\theta^{\alpha'}|^2\rangle\Big)_{\tau=0} < 0 \tag{34a}$$

provided that

$$\langle\beta_{\alpha}{}^2\rangle > \langle\beta_{\alpha}{}^{2'}\rangle. \tag{34b}$$

[3] Malkus and Veronis assume perturbations in w and θ have the form, Aw', and $B\theta'$. However, in the limit $\sigma \to \infty$, it follows from (7) that $A=B$.

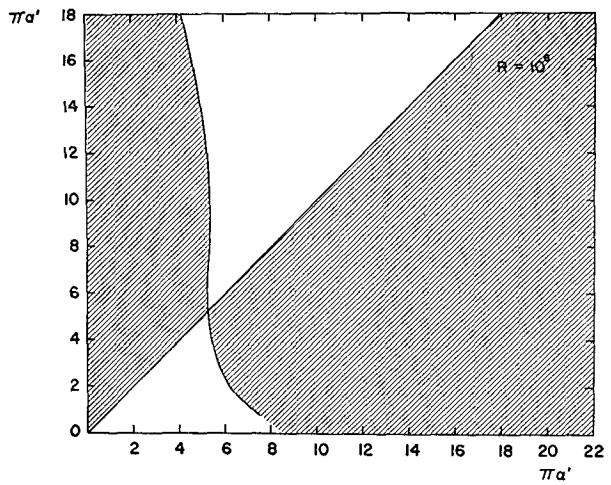

FIG. 16. Stability diagram for $R=10^6$. α is the wave number that supports the convection and α' is the wave number of the small perturbation.

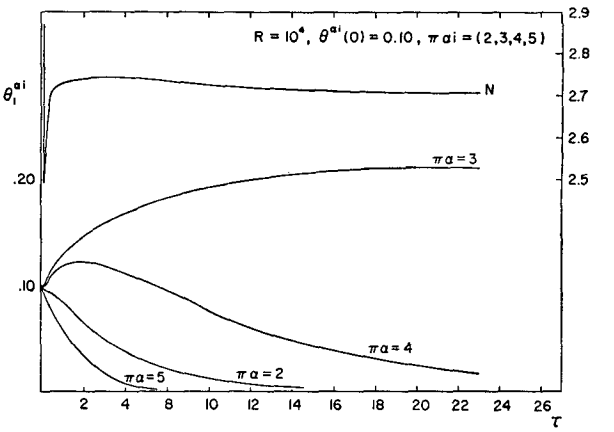

FIG. 17. The development of a four wave number system to steady state. The figure shows the evolution of the first sine modes of the temperature fluctuation fields, θ_1^{α}, and the evolution of the total heat transport, N. The Rayleigh number and the values of α are given in the figure.

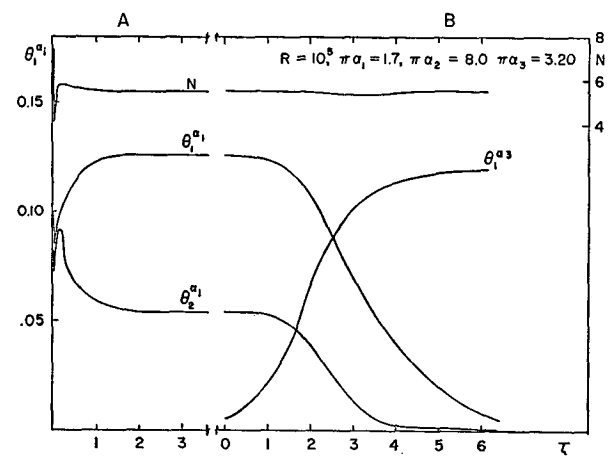

FIG. 18. (a) The development of a double-α system, $\pi\alpha_1=1.7$, $\pi\alpha_2=8.0$, to steady state. The figure shows the evolution of the first sine modes of the temperature fluctuation field, θ_1^{α}, and the evolution of the total heat transport. The scale for N is to the right of the figure. (b) The development of the system comprised initially of the steady state form of the double-α system described in Fig. 18a, plus a small perturbation at $\pi\alpha_2=3.20$.

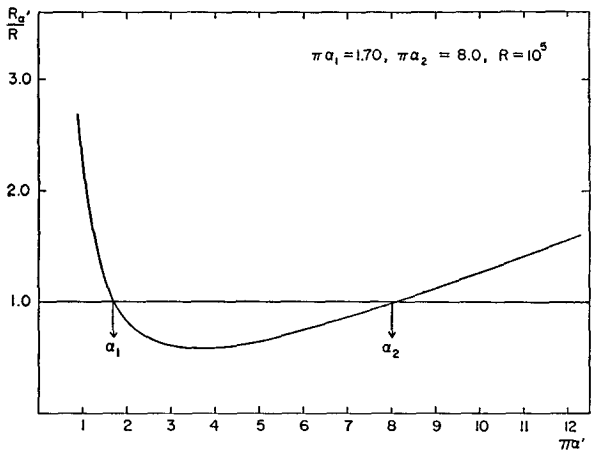

FIG. 19. Critical Rayleigh number, $R_c(\alpha)$ for the system described in Fig. 18a. The two values of α which support the convection are designated as α_1 and α_2.

For the proof of conditions (34), we refer the reader to the papers of Malkus and Veronis (1958), and Malkus (1954).

In order to prove relative stability one would have to show that (34b) is a sufficient condition for (34a) not only for $\tau=0$ but also for all times subsequent to $\tau=0$. If such a proof could be made, we would have found that the stable solutions were also those which maximize $\langle\beta^2\rangle$. Since this is not so, we may conclude that if the stable solution is introduced as a small perturbation on the one that maximizes $\langle\beta^2\rangle$, it will initially decrease, in conformity with inequalities (34), but will later increase and dominate the convection, and the mode that maximizes $\langle\beta^2\rangle$ will decay to zero amplitude. This is indeed the case, as is illustrated in Fig. 20. This figure shows the initial development of $\langle|\delta\theta^{\alpha_2}|^2\rangle$ for a small perturbation $\delta\theta^{\alpha_2}$ subsequent to its introduction into the system, $\theta^{\alpha_1},\beta_{\alpha_1}$, which maximizes $\langle\beta^2\rangle$. The initial form of $\delta\theta^{\alpha_2}$ is that of the stable solution found from the linear analysis with the initial amplitude reduced by a factor of 100. The value of R and the wave numbers α_1 and α_2 are given in the figure caption. We note that after the initial decrease predicted by (34), $\langle|\delta\theta^{\alpha_2}|^2\rangle$ increases sharply. A continuation of the calculation for $\tau>0.1$ shows that $\delta\theta^{\alpha_2}$ eventually grows to full amplitude while θ^{α_1} decreases to zero. The behavior of the α_2 mode shown in the figure is entirely in the linear regime; the amplitudes θ^{α_1} and β_{α_1} remain constant to one part in 10^4 for $\tau<0.3$.

The failure of the relative stability criterion stems from the fact that the small disturbance at wave number α' is adequately represented by the form $A\theta^{\alpha'}$ only immediately after its introduction into the system. At any finite time after introducing the disturbance it contains components linearly independent of $\theta^{\alpha'}$, which are excited by the interaction of $\theta^{\alpha'}$ with the mean-distorted temperature field. These components either return amplitude to $\theta^{\alpha'}$ or drain more amplitude from it. Which of these alternatives happens depends sensitively on the detailed shape of mean temperature field, and apparently cannot be inferred from a knowledge of only a single moment such as $\langle\beta^2\rangle$.

5. Discussion of results and conclusions

The results presented in Section 4 appear to have the correct qualitative behavior in many respects. The sharp boundary layering of the mean temperature field at large Rayleigh numbers, and the $R^{\frac{1}{2}}$ law for the Nusselt number which was recovered by the calculation are consistent with the supposition that a large part of the dynamics of convection is contained in the fluctuating mean interactions, together with the self-distortion of the mean temperature field produced by the motions themselves. On the other hand, there are certain respects in which the non-fluctuating system appears to be unrealistic. Thus, the stable amplitudes are steady in time, and contain only one horizontal wave number. In addition, the Nusselt number is independent of the Prandtl number, σ, so that the system can be realistic only for $\sigma\to\infty$.[4] In the following paragraphs we shall discuss in detail the realism of the non-fluctuating system.

The most satisfactory way of assessing the realism of the nonfluctuating system would be to introduce a realistic approximation for the fluctuating terms into the equations of motion and compare the answers for the resulting system to the present calculation. At present, we have only preliminary results for such a comparison at large $\sigma(\sigma\to\infty)$. The temperature fluctuation field was represented by three amplitudes $\theta^{\alpha_1}(z)$, $\theta^{\alpha_2}(z)$, and $\theta^{\alpha_3}(z)$. The wave vectors α_i formed a closed triangle, and all couplings among the θ^{α_i} prescribed by the last term of equation (2) were retained (in both the vertical and horizontal). The heat transport for this calculation (at $R=10^6$) is within about 10 per cent of that found for the nonfluctuating system. This representation of the fluctuating interactions is crude, and we mention it here only to indicate the order of magnitude of the estimated error at large σ.

A direct test of the realism of the nonfluctuating system is to compare it to experiment. The most important single quantity it should correctly predict is the Nusselt number, and its dependence on the Rayleigh number. We may also compare to experimental data its predictions for the mean temperature field, $\bar{T}(z)$, and for the horizontally averaged rms temperature and velocity fluctuations, $\tilde{\theta}(z)$ and $\tilde{w}(z)$, and $\bar{T}$. For the Nusselt number there exist fairly accurate experiments with which the results may be compared. As for $\tilde{\theta}$, $\tilde{w}$, and $\bar{T}$, we must relay on the less quantitative mixing length estimates, because of the lack of experimental data. In making the comparison with experiments, we choose those data for which σ is as large as possible.

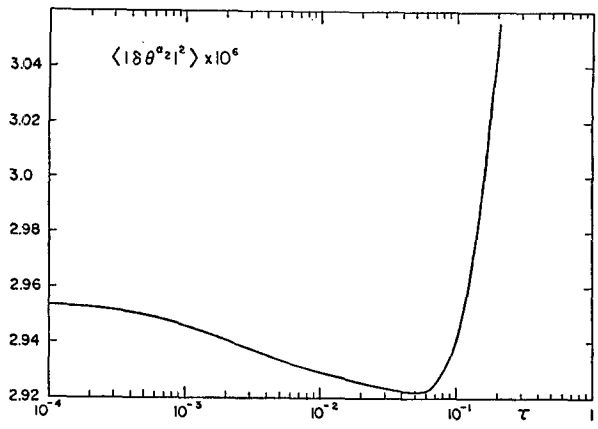

FIG. 20. Test of the relative stability criterion. The figure shows the initial development of the mean squared temperature fluctuation, $\langle|\delta\theta^{\alpha_2}|^2\rangle$, for a small disturbance $\delta\theta^{\alpha_2}$ whose form is that of the stable solution. The disturbance $\delta\theta^{\alpha_2}$ is introduced as a small perturbation into the system which maximizes $\langle\beta^2\rangle$. The initial amplitude of $\delta\theta^{\alpha_2}$ is 100 times smaller than its steady state value.

Experimental data for the total heat transport are available for fluids of large Prandtl number, σ. Globe and Dropkin (1959) and Silveston (1958) have measured the convective heat transport for silicone oils, as well as for other fluids. The range of σ for the experiments of Globe and Dropkin extended up to $\sigma=8750$, while Silveston's measurement extended to $\sigma=3000$. At large R, Globe and Dropkin report a value of $N/R^{\frac{1}{3}}=0.134$, at $\sigma=8750$. Silveston's data at large σ ($5\lesssim\sigma\lesssim3000$) is well represented by $N/R^{\frac{1}{3}}\cong0.09$. Actually, Silveston fits his data by the power law, $N\simeq0.10\ R^{0.31}\ \sigma^{0.05}$, and Globe and Dropkin represent their data by $N\simeq0.069R^{\frac{1}{3}}\sigma^{0.074}$. The Prandtl number dependence given by the above formulas is none too certain, especially at very large σ. At sufficiently large σ, we expect N to be independent of σ. This follows from an inspection of the nondimensional equations of motion (1)–(4). Above what value of σ the σ dependence of N disappears is not yet known, but the mixing length estimates of Kraichnan (1962) suggest it to be at $\sigma\sim300$.

In comparing the above experimental data to the numerical calculations, we shall select those solutions which are stable against small perturbations. This choice appears to be most natural, since the nonfluctuating system possesses its own stability properties, and

[4] See Kraichnan (1962, p. 1377 *et seq.*) for a discussion of this point.

requires no additional constraints such as maximum heat transport or maximum $\langle\beta^2\rangle$ to make its dynamics complete. For these solutions, the heat transport at large R is given by

$$N=0.1153R^{\frac{1}{3}}. \tag{35}$$

Actually, the use of N_{max}, given by equation (28) or the N which characterizes those solutions which maximize $\langle\beta^2\rangle$ as given by equation (29) would not significantly change the numerical comparison. We observe that N as given by (35) is about 17 per cent smaller than the experimental results of Globe and Dropkin, and about 20 per cent larger than the results of Silveston for large σ fluids.

With regard to the profiles, $\bar{T}(z)$, w(r), and Θ(r), there are, unfortunately, not many accurate data with which to compare them. The only experimental data for the profiles are those of Townsend (1959), who measured them for air ($\sigma=0.74$). Townsend did not have an upper boundary in his experiment, so that it is not clear how to compare his measurements with the present calculation. He found that the experimental data outside the boundary—which had considerable scatter—was best fit by a z^{-1} law for $\frac{1}{2}-\bar{T}$ and a $z^{-0.6}$ law for θ.

On the other hand, Kraichnan (1962) has made mixing length calculations of the profiles for arbitrary σ. For large σ, he finds $\frac{1}{2}-\bar{T}\sim z^{-1}$, $w\sim z$, and $\theta\sim z^{-1}$, provided z is larger than the thickness of the conduction boundary layer, 0.5/N, but less than the viscous boundary 6.4 $\sigma^{\frac{1}{3}}$/N. For sufficiently large σ the latter exceeds the distance between the conducting plates. Kraichnan furthermore estimates that for air ($\sigma=0.74$), the z^{-1} regime is so thin that it may be difficult to observe experimentally.

The rms values of the fluctuating fields w, and θ computed here may be represented by the following power laws outside the conduction boundary layer:

$$\tilde{w}(Z)\cong 0.15R^{\frac{1}{3}}z \tag{36}$$

$$\tilde{\theta}(Z)\cong 0.78\frac{1}{R^{\frac{1}{3}}z}. \tag{37}$$

The above formulas were obtained by fitting the numerical profiles exterior to the boundary layer by power laws. Their accuracy is $\sim$10 per cent for $0.1<z<0.3$, and for $R\geq 10^5$. The powers of R in (36) and (37) are not determined with great accuracy by the numerical fitting procedure. Their validity appears to be approximately $1/N\lesssim Z\lesssim\frac{1}{3}$. We observe that (36) and (37) are consistent with Kraichnan's mixing-length estimates. They appear to have the same dependence on R, and the numerical coefficients also appear to be consistent with his. His numerical values of the coefficients in (36) and (37) are 0.095 and 0.96, respectively. The numerical discrepancy is due in part to the fact that Kraichnan estimates the value of $N/R^{\frac{1}{3}}$ as 0.089.

The computed mean temperature profile, $\bar{T}(z)$, has generally the correct form but $\frac{1}{2}-\bar{T}$ does not follow a z^{-1} law, as predicted by Townsend's data, and by the mixing-length estimates of Kraichnan. The z^{-1} behavior is prevented by the development of a thin stabilizing layer [$\beta(z)<0$] just exterior to the thermal boundary layer. Beyond the stabilizing layer, β becomes positive, and $\frac{1}{2}-\bar{T}$ apparently may follow a Z^{-1} law, at large R. This is indicated by preliminary analytic studies of the nonfluctuating system and is suggested by an examination of the numerical calculations. However this behavior beyond the stabilizing layer is probably only qualitatively correct; the mixing-length estimates indicate that $-\bar{T}+\frac{1}{2}\sim\theta$, whereas our numerical calculations at $R=10^6$ have $-\bar{T}+\frac{1}{2}\sim 4\times 10^{-3}\theta$ for values of z larger than the boundary layer thickness.

We interpret the presence of a stabilizing region ($\beta<0$) in the mean temperature profile as an explicit result of the omission of the fluctuating interactions. Its role in the dynamics of the nonfluctuating system is to quench the development of large scale motions which absorb relatively large amounts of heat from the lower boundary and lose little of their buoyancy and momentum by molecular dissipation. If the fluctuating interactions had been included, the presence of such a region would not be necessary, because the large scale motions would lose their temperature excess and momentum by eddy conductivity and eddy viscosity.

The existence of a stabilizing region for the nonfluctuating system is necessary if the Nusselt number follows a $R^{\frac{1}{3}}$ law at large R. This may be seen by the following argument. If we assume that the mean temperature gradient, $\beta(z)$, is known, we may regard the steady state equations satisfied by w and θ as an eigenvalue problem for the determination of R as a function of $N=\beta(0)$. This problem is the same as the linear stability problem with $\alpha'=\alpha$, and may be solved by the technique given in Section 4b. We note that as the problem is posed, R is a function of the α which supports the motion, so that for a fixed N one chooses that α for which R is minimum, in order to achieve stability. We may now ask what features $\beta(z)$ must have in order to obtain $N\sim R^{\frac{1}{3}}$. If $\beta(z)$ is positive throughout the region of convection, one may show, using the methods of IV b, that $N\sim R^{\frac{1}{3}}$, for any reasonably choice for $\beta(z)$. Hence, we may conclude that an $R^{\frac{1}{3}}$ law is incompatible with an entirely positive β for the nonfluctuating system. If we permit β to be negative, we may obtain an $R^{\frac{1}{3}}$ law by judiciously choosing the extent and magnitude of the negative β region.

In conclusion, we may infer from the above discussion that the nonfluctuating system has reasonably good quantitative accuracy for the total heat transport, N, for large Prandtl number fluids. We are prevented from drawing definite conclusions about the exact magnitude of its error by the lack of self-consistent experimental

data at large σ. Preliminary numerical estimates of the influence of the fluctuating self-interactions on the total heat transport suggest that the nonfluctuating system is in error by about 10 per cent for $\sigma\to\infty$.

The rms values of the fluctuating amplitudes, w and Θ, appear to be consistent with the mixing length estimates of Kraichnan. This fact is somewhat surprising in that the mixing-length theory assumes—exterior to the boundary layer—that the fluctuating mean interaction is balanced by the fluctuating interactions. Our procedure omits the latter entirely. Perhaps the nonlinearities in the nonfluctuating system are self-compensating in this respect.

The most obvious unrealistic feature of the system is the overshoot region in the mean temperature field. As stressed above, this behavior can be removed only by the introduction of estimates for eddy processes into the equations of motion.

Acknowledgments. I wish to thank Dr. R. H. Kraichnan for many illuminating discussions throughout the completion of this work and the preparation of this manuscript. I am also grateful to Dr. W. V. R. Malkus and Dr. E. A. Spiegel for the many valuable discussions regarding their own theoretical approaches to the convection problem and for their useful comments on a final version of the manuscript.

It is a pleasure to acknowledge the able assistance of Mr. R. Rustin who programmed and carried out the numerical computations on the IBM 7094.

APPENDIX

In this section we compute the rigid boundary Green's function, $G(z|z')$ and its sine-transform matrix, $G_{n,m}$.[5] $G(z|z')$ satisfies

$$\left(\frac{d^2}{dz^2}-\pi^2\alpha^2\right)^2 G(z|z')=\pi^4\delta(z-z') \tag{A1}$$

with the boundary conditions,

$$G_r(0|z')=\frac{\partial G}{\partial z}(0|z')=0,$$
$$G_r(1|z')=\frac{\partial G}{\partial z}(1|z)=0. \tag{A2}$$

For free boundaries, the corresponding Green's function, $G_f(z|z')$ is conveniently represented by a sine series:

$$G_f(z|z')=2\sum_1^\infty \frac{\sin n\pi z \sin n\pi z'}{(n^2+\alpha^2)^2}. \tag{A3}$$

Since G_r and G_f satisfy the same differential equation, they differ only by the homogeneous solution to (A1):

$$G_r(z|z')=G_f(z|z')+A(z')\sinh\pi\alpha z + B(z')\sinh\pi\alpha z+C(z')z\cosh\pi\alpha z. \tag{A4}$$

The coefficients A, B, and C are obtained by demanding that G_r, as given by (A4), satisfies the boundary conditions (A2). Denoting the homogeneous solution by $y(z|z')$, we find

$$y(z|z')=\frac{1}{\Delta}\frac{\partial G_f}{\partial z}(0|z')\{\pi\alpha(1-z)\sinh\pi\alpha z - z\sinh\pi\alpha\sin\pi\alpha(1-z)\}$$
$$+\frac{1}{\Delta}\frac{\partial G_f}{\partial z}(1|z')\{-\pi z\sin\pi\alpha(1-z) + (1-z)\sinh\pi\alpha\sinh\pi\alpha z\}$$

where

$$\Delta=\sinh^2\pi\alpha-\pi^2\alpha^2. \tag{A5}$$

The derivatives of G_f occurring in (A5) may be computed from (A3). Using (A5), (A4), and (A3), we may compute the matrix $G_{n,m}$. The result is given by equation (17).

[5] The calculation of G presented here is similar to a corresponding calculation in the stability of Couette flow. See Chandrasekhar (1962, p. 300 *et seq.*).

REFERENCES

Chandrasekhar, S., 1961: *Hydrodynamic and hydromagnetic stability*. Oxford, Clarendon Press, p. 16.

Globe, S., and D. Dropkin, 1959: Natural convection heat transfer in liquids confined by two horizontal plates and heated from below. *J. heat Transfer*, **81**, 24–28.

Herring, J. R., 1963: Investigation of problems in thermal convection. *J. atmos. Sci.*, **20**, 325–338.

Hildebrand, F. B., 1952: *Methods in applied mathematics*. Englewood Cliffs, N. J., Prentice-Hall, Inc., p. 66 *et seq.*

Kraichnan, R. H., 1962: Turbulent thermal convection at arbitrary Prandtl number. *Phys. Fluids*, **5**, 1374–1389.

Malkus, W. V. R., 1954: The heat transport and spectrum of thermal turbulence. *Proc. Roy. Soc. London*, A, **225**, 196–212.

——, 1959: Magnetoconvection in a fluid of infinite electrical conductivity. *Astrophys. J.*, **130**, 259–275.

——, 1960: Outline of a theory of turbulent convection. *Theory and fundamental research in heat transfer*, London, Pergamon Press, p. 203–212.

——, and G. Veronis, 1958: Finite amplitude cellular convection. *J. fluid Mech.*, **4**, 225–260.

Silveston, P. L., 1958: Wärmedurchgang in waagerechten Flüssigkeitsschichten. *Forsch. Gebiete Ingenieurw.*, **24**, 59–69.

Spiegel, E. A., 1962: On the Malkus theory of turbulence. *Mechanique de la Turbulence*, Paris, C.N.R.S., 181–201.

Townsend, A. A., 1959: Temperature fluctuations over a heated horizontal surface. *J. fluid Mech.*, **5**, 209–241.